Vertical structure of low-frequency currents in the southwestern East Sea (Sea of Japan)

Article *in* Journal of Oceanography · April 2009

DOI: 10.1007/s10872-009-0024-x

5 authors, including:

Kyung-Il Chang
Seoul National University
61 PUBLICATIONS **1,402** CITATIONS
SEE PROFILE

Jae Hak Lee
Korean Institute of Ocean Science and Technology
67 PUBLICATIONS **1,318** CITATIONS
SEE PROFILE

Journal of Oceanography, Vol. 65, pp. 259 to 271, 2009

Vertical Structure of Low-Frequency Currents in the Southwestern East Sea (Sea of Japan)

YUN-BAE KIM[1], KYUNG-IL CHANG[1]*, KUH KIM[1], JAE-HUN PARK[2] and JAE-HAK LEE[3]

[1]*Research Institute of Oceanography/School of Earth and Environmental Sciences, Seoul National University, Seoul 151-742, Korea*
[2]*Graduate School of Oceanography, University of Rhode Island, Narragansset, RI 02882-1197, U.S.A.*
[3]*Climate Change and Coastal Disaster Research Department, Korea Ocean Research and Development Institute, Ansan 425-600, Korea*

(Received 6 May 2008; in revised form 16 September 2008; accepted 17 November 2008)

The vertical structure of low-frequency flows in the central Ulleung Interplain Gap of the southwestern East Sea (Sea of Japan) is analyzed based on full-depth current measurement during November 2002–April 2004. Record-length mean flows are directed toward the Ulleung Basin (Tsushima Basin) throughout the entire water column. Upper current variability above the permanent thermocline with a dominant period of about 50–60 days is shown to be closely related to the displacement of an anticyclonic warm eddy associated with the westward meander of the Offshore Branch. Fluctuations of deep currents below the permanent thermocline have a dominant period of about 40 days. Coherence between the current near the seabed and shallower depths is statistically significant up to 360 m for a period range between 15 and 100 days, but less significantly correlated with currents in the upper 200 m. Data from the densely equipped mooring line reveal that mean and eddy kinetic energies are minima at 1000 m, where isotherm slopes are also relatively flat. Empirical orthogonal function (EOF) analyses suggest that more than 79% of total variances of upper and deep currents can be explained by their respective first EOF mode characterized by nearly depth-independent eigenvectors. Spectral and EOF analyses of observed currents suggest that most of the deep current variability is not directly related to local upper current variability during the observation period.

Keywords:
· Sea of Japan,
· moored current observation,
· low-frequency current variability,
· vertical structure of current.

1. Introduction

The East Sea[§] is a semi-enclosed marginal sea in the northwestern Pacific. The sea consists of three basins deeper than 2000 m: the Japan Basin (JB), the Ulleung Basin[¶] (UB), and the Yamato Basin (Fig. 1). The Ulleung Interplain Gap[†] (UIG), located in the southwestern East Sea, is approximately 90 km wide, and is a nearly symmetric, deep channel with a maximum depth of approximately 2300 m at its southwestern tip. Deep water is formed in the JB (Kim *et al*., 2004), leading to a thermohaline circulation that transports deep, cold water toward the southern basins. The Korea Plateau, which is shallower than 1500 m, lies between the JB and UB, whereas the Oki Spur, which is shallower than 500 m, acts as a barrier to deep water exchange between the UB and Yamato Basin. Thus, the UIG serves as a passageway for the exchange of deep waters below 1500 m between the UB and the JB (Kim *et al*., 1991). Direct measurement of currents through the UIG would provide useful information to help us understand the thermohaline circulation of the East Sea and deep circulation in the UB.

The Subpolar Front (SPF), which is a strong thermal boundary in the central part of the East Sea, separates the southern warm water region from the northern cold water region. Mitchell *et al*. (2005b) reported that the SPF frequently forms a large meander trough within the UIG and oscillates in an east-west direction with a period of approximately 60 days. The SPF meander allows cold water north of the SPF to be brought into the UB. Upper circulation in the UB south of the SPF is affected mainly

* Corresponding author. E-mail: kichang@snu.ac.kr

§ The Editor-in-Chief does not recommend the usage of the term "East Sea" in place of "Sea of Japan" or "Japan Sea".

¶The Editor-in-Chief does not recommend the usage of the term "Ulleung Basin" in place of "Tsushima Basin".

†The "Ulleung Interplain Gap" corresponds to the "Oki Gap".

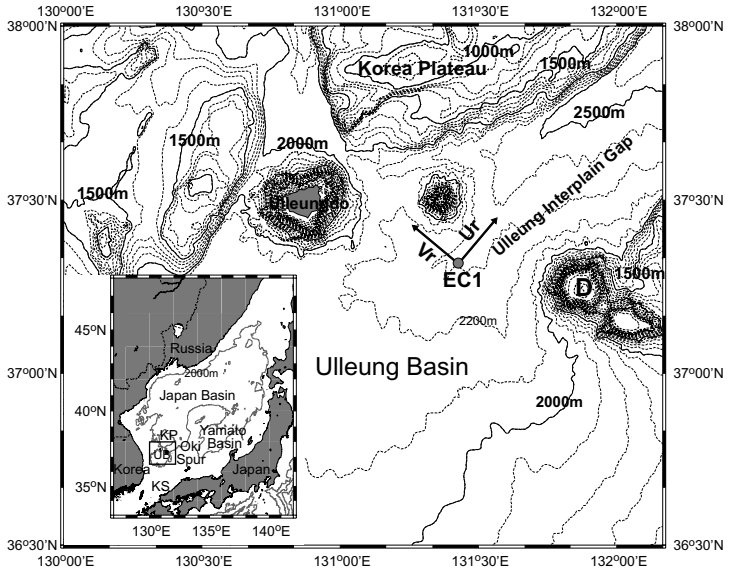

Fig. 1. Topography of the Ulleung Interplain Gap[†]. Isobaths are drawn every 100 m. Arrows indicate the along-channel (Ur) and cross-channel (Vr) directions. Inset map shows the East Sea[§] with 2000 m isobath contour. KP, UB, and KS denote the Korea Plateau, Ulleung Basin[¶], and Korea Strait, respectively.

by the Tsushima Warm Current (TWC) through the Korea Strait, its northward branch along the east coast of Korea (the East Korean Warm Current, EKWC), and its northeastward branch along the outer edge of the Japanese continental shelf (the Offshore Branch, OB). The OB sometimes extends farther to the north along the Oki Spur, reaching 37°30′ N (Mitchell *et al*., 2005a).

When the EKWC separates from the coast at approximately 37.5°N, part of it meanders to the southwest and contributes to the formation of the anticyclonic Ulleung Warm Eddy (UWE) centered near Ulleungdo (Chang *et al*., 2004). A small-scale cyclonic cold eddy, the Dok Cold Eddy, is often pinched off from the meandering trough of the EKWC, and either resides south of Dokdo[‡] (D in Fig. 1) or migrates to the west (Mitchell *et al*., 2005b). Conductivity-temperature-depth (CTD) data taken in the UIG frequently show a tilting of isotherms sloping upward to the eastern UIG, indicative of the southward geostrophic upper currents in the UIG due to the meandering of EKWC and the UWE (Chang *et al*., 2002b). However, few continuous direct current measurements have been made in the UIG to quantify the upper currents and variability.

Since November 1996, a subsurface current meter mooring line has been in operation at a midpoint site of the UIG (site EC1 in Fig. 1) to monitor the deep flow and its variability (Chang *et al*., 2002a, 2004). Site EC1 is the longest-running current meter mooring site in the East Sea. The mooring at EC1 has been typically equipped with three current meters at around 400 m, 1400 m, and 20 m above the seabed. Data from EC1 show that deep currents flow mainly southwestward with a dominant period of 20–50 days (Chang *et al*., 2004). Upper currents were also measured at EC1 for about 7 months from October 2001 to May 2002, showing that mean currents in the upper layer are also directed into the UB, to the southeast in the upper 130 m, and to the southwest below 370 m (Chang *et al*., 2004). The relationship of the variability of deep flow to that of the upper layer, however, was not exhaustively discussed because Chang *et al*. (2004) focused on providing an overview of upper and deep circulation in the entire UB.

An array of five current mooring lines, including the mooring at EC1, was deployed in the UIG for 16.5 months from November 2002 to April 2004. The mooring line at EC1 was instrumented to cover the full water column, making it the first current measurement to concurrently observe both the upper and deep layers for more than one year in the UB. This paper describes the characteristics of observed currents and vertical structure of current fluctuations over the entire water column at EC1 based on data from the full-depth moored current measurements for 16.5 months. We define the layer between the surface and 200 m as the upper layer, and that between 360 m and near the sea floor as the deep layer. The 200 m depth approximately corresponds to the base of the permanent thermocline in the UB and UIG (Chang *et al*., 2002b) (see also Fig. 7).

[‡]The Editor-in-Chief does not recommend the usage of the term "Dokdo" or "Dok Island" in place of "Take Shima".

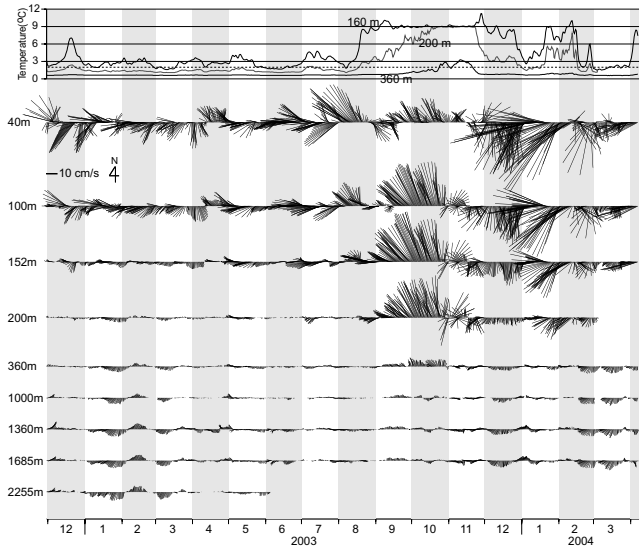

Fig. 2. Vector time series of low-pass filtered currents during November 2002–April 2004 at EC1. Current data obtained by an acoustic Doppler current profiler, available between 40 and 152 m at 4 m intervals, are shown at only three depth levels, 40, 100, and 152 m. Current at other depth levels were measured by RCM current meters. Time series of measured temperature at selected depths are shown in the uppermost panel with a dashed line at 2°C, which represents the lower boundary of the permanent thermocline.

2. Data and Methods

The full-depth current meter mooring at EC1 was equipped with an upward-looking acoustic Doppler current profiler (ADCP, RDI WHS300) at 160 m and six Aanderaa RCM-7 and RCM-8 current meters at 200, 360, 1000, 1360, 1685, and 2255 m, the deepest current meter being placed 20 m above the sea floor. The ADCP recorded current profiles every hour from the surface to near the mooring depth with 4-m vertical resolution. The accuracy of measured velocity and direction is ±0.5% of the measured velocity and ±2°, respectively. For this analysis we used only the ADCP data at and below 40 m because the near-surface data are mostly erroneous. Temperature was also measured at the ADCP mooring depth by the built-in temperature sensor. The RCMs recorded current speed, current direction, temperature, and pressure every 30 min at each mooring depth. The accuracy of the current speed and temperature is ±4% of actual speed, and ±0.05°C, respectively. Because of a power failure, the current meter near the seabed yielded only 6 months of data from the start of the mooring. The data return at 200 m was approximately 1 month shorter than the entire observation period, and the data gap at 200 m was filled by a linear interpolation using current data at adjacent depths of 152 and 360 m. Data processing for stall periods of the RCMs was the same as that used by Teague *et al*. (2005).

Current and temperature data are low-pass filtered with a 40-h Hanning cosine filter to remove tidal and inertial motions and subsampled at 12-h intervals. Considering the orientation of the UIG, the low-pass filtered current data are decomposed into along-channel (Ur, 50° clockwise from north) and cross-channel (Vr) components (Fig. 1). Vector time series of low-pass filtered currents at selected depths and time series of Ur and Vr components are shown in Figs. 2 and 3, respectively.

In order to examine the predominant vertical structure and its temporal variation, empirical orthogonal function (EOF) analyses are performed separately for the Ur and Vr velocity components. Kundu *et al*. (1975) outlined the EOF method, and Overland and Preisendorfer (1982) suggested a Monte Carlo experiment to determine the significance of EOF modes. If λ_n, $n = 1, 2, ..., N$, represents the eigenvalues, then the normalized eigenvalue T_n is

$$T_n = \lambda_n \left(\sum_{n=1}^{N} \lambda_n \right)^{-1}, \quad n = 1, 2, ..., N.$$

If δ_n^r, $n = 1, 2, ..., N$ is the set of eigenvalues produced by the r-th Monte Carlo experiment, the statistic analogous to T_n is

$$U_n^r = \delta_n^r \left(\sum_{n=1}^{N} \delta_n^r \right)^{-1}, \quad n = 1, 2, ..., N, \quad r = 1, ..., 100.$$

The significant EOF modes are determined by the values of T_n/U_n^{95} if this ratio exceeds 1 according to Rule N (Preisendorfer, 1988). We describe only the significant EOF modes. Moreover, to determine whether adjacent EOF modes are distinguishable, the standard error of the eigenvalues is also estimated by $\Delta\lambda = \lambda\sqrt{2 / N^*}$ where λ is the eigenvalue and N^* is the number of realizations (North *et al*., 1982).

3. Results

3.1 Subsurface temperature and upper currents

The uppermost panel of Fig. 2 shows time series of temperature at 160, 200, and 360 m depths. The lower boundary of the permanent thermocline is considered to be 2°C in the UB and UIG, below which relatively homogeneous water masses with temperature <1°C are found (Chang *et al*., 2002b) (see also Fig. 7). Temperature time-series indicate that the depth of the 2°C isotherm lay mostly between 160 and 200 m before mid-August 2003, while it was located mostly below 200 m depth afterwards

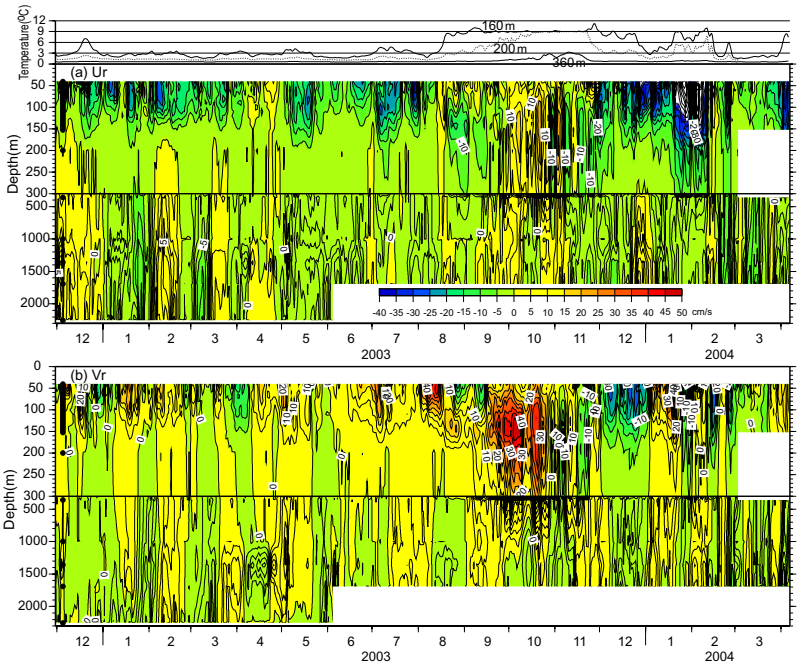

Fig. 3. Time series of (a) along-channel (Ur) and (b) cross-channel components (Vr) for low-pass filtered currents during November 2002–April 2004. Positive Ur and Vr are directed to northeast and northwest, respectively. The contour interval in the upper 300 m and below 300 m is 5 cm/s and 1 cm/s, respectively, whereas, the color scale is the same over the full water column. Depths of available current data are shown (black dots) at the left side of each figure. Time series of water temperature at selected depths are shown in the upper panel.

and found even deeper than 360 m between late October and mid-November 2003 (Fig. 2). Thus, the current meter at 200 m was located below the permanent thermocline during the first half of the entire mooring period, but was mostly within the permanent thermocline during the second half.

One remarkable observation is the variability of the upper currents, changing in association with changes in subsurface temperature (Fig. 2). Subsurface temperature before mid-August 2003 showed small fluctuations of about 2–5°C at 160 m, and temperature at 200 m remained below 2°C, except for a sudden increase by about ~5°C at 160 m in mid-December 2002 for approximately 1 week. Temperature increased sharply by 6°C at 160 m within 10 days in mid-August 2003 and remained at 9°C for 3 months from late August to late November 2003. We call this period from mid-August to late November 2003 the first warming event hereafter. During the period of the first warming event, temperature at 200 m also gradually increased by about 7°C from mid-August to October 2003 and became the same as the temperature at 160 m from mid-October to late November, after which temperature at both depths started to decrease. Hence, an isothermal layer formed from at least 160 to 200 m between mid-October and late November, and temperature at 360 m achieved a maximum value during this period.

Before the first warming event, currents between 40 and 360 m were mainly directed to the southwest (Fig. 2). Northwestward currents at 40 and 100 m shown in Fig. 2 strengthened before the start of the first warming event in early August 2003, and the gradual increase in temperature at 200 and 360 m was accompanied by an abrupt strengthening of northwestward flows between 100 and 360 m, which persisted for approximately 2 months until late October 2003. During this period, currents at 152 m were stronger than currents at shallower depths with a maximum speed of 52 cm/s, and currents at 40 m were weaker than those between 100 and 200 m. Upper currents became weak and variable afterwards during the period when temperature between 160 and 200 m was isothermal and temperature at 360 m was at its maximum over the entire mooring period.

At 160 m, temperature gradually decreased with about 10-day fluctuations until the beginning of January 2004, when it was 3°C, a similar temperature value to that before the start of the first warming event. The decrease in temperature also occurred at 200 m, but with a sharp drop in late November 2003. During this cooling period, strong southward currents emerged with a maximum speed at 40 m, decreasing with depth.

After showing a local minimum in early January 2004, temperature again increased by about 6°C at 160 m

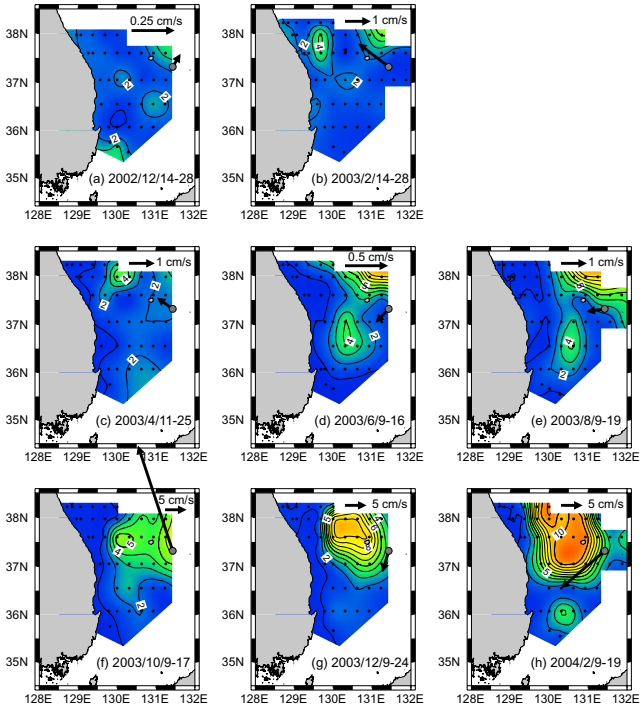

Fig. 4. Bimonthly horizontal distributions of temperature at 200 m between December 2002 and February 2004. Dots and grey circle denote CTD stations and mooring location EC1, respectively. The contour interval of temperature is 1°C. The 8-day averaged mean current vectors at 200 m observed at EC1 around the time of CTD observation at nearest station to EC1 are also shown. Note the different scale bars for the current vectors. (CTD data source: National Fisheries Research and Development Institute of Korea).

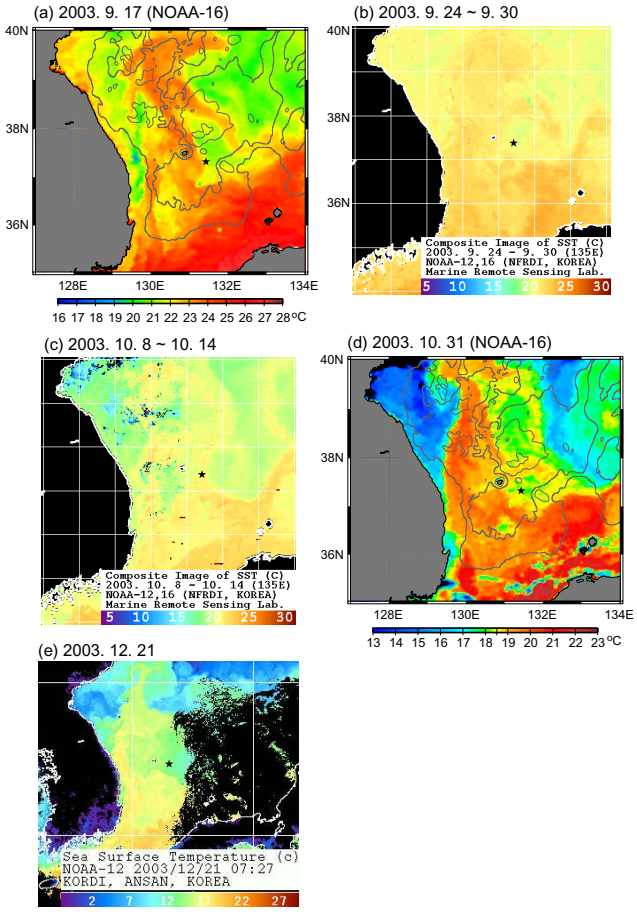

Fig. 5. Satellite-derived sea surface temperature images taken (a) on September 17, 2003, (b) between September 24 and September 30, 2003, (c) between October 10 and October 14, 2003, (d) on October 31, 2003, and (e) on December 21, 2003. Solid star shows the location of EC1. Isobaths at 1000 m intervals are shown in (a) and (d). (Data or figure source: (a) and (d), from http://www.nodc.noaa.gov/, (b) and (c), from http://www.nfrdi.re.kr/, and (e) from http://www.kordi.re.kr/)

and by about 4°C at 200 m in mid-January 2004, the second warming event persisted for about 1 month between mid-January and mid-February. The second warming event was accompanied by strong southwestward flows with a maximum speed of 78 cm/s at 40 m.

The observed subsurface temperature and current variations, especially during the first warming event, suggest that anticyclonic warm eddy features swept through the mooring site EC1 from east to west. Figures 4(a)–(h) show the bimonthly horizontal distribution of temperature at 200 m based on CTD data obtained by the National Fisheries Research and Development Institute of Korea during the mooring period. Each hydrographic survey was completed within 8–15 days. Shown in Fig. 4 are 8-day averaged mean current vectors at 200 m at EC1 around the time of CTD observation at the nearest station from EC1. The 8-day averaging period is based on an integral timescale of 7 days for the dominant velocity component, Ur, at 200 m.

In December 2002 and February and April 2003, the UB area at 200 m was filled with cold water <4°C, and currents at 200 m were weak with mean speed less than 1.5 cm/s (Figs. 4(a)–(c)). In June and August 2003, a warm water region with temperature higher than 8°C appeared around 38°N. The mooring site, however, was located outside the steep temperature gradient, and currents at 200 m were still weak (Figs. 4(d) and (e)). Observed current directions coincided roughly with those inferred from the horizontal temperature gradient with higher temperature north of EC1, except for December 2002. The warmest water region with temperature higher than 6°C was located around EC1 in the survey area in October 2003 (Fig. 4(f)). A strong northwestward current with a mean speed of 26 cm/s was observed at 200 m at EC1. Tem-

Table 1. Basic statistics of low-pass-filtered currents at 12-hourly intervals at EC1 for November 2002–April 2004 (record-length), November 2002–early August 2003 (first half) and early August 2003–April 2004 (second half). All directions are measured clockwise from the north. Ur and Vr denote along-channel and cross-channel components of currents, respectively. SD, MKE, and EKE denote the standard deviation, mean kinetic energy, and eddy kinetic energy, respectively.

Period	Mooring depth	Velocity component	Mean	SD	Vector mean			MKE	EKE	EKE/MKE	Principal axis	Direction stability
					Speed	Dir.	Max. speed					
	(m)		(cm/s)	(cm/s)	(cm/s)	(°)	(cm/s)	(cm^2/s^2)	(cm^2/s^2)		(°)	
Record-length	40	Ur	−12.0	16.3	12.6	248	78.7	79.1	240.7	3.0	42	0.6
(2002/11/30–2004/4/7)		Vr	3.9	14.7								
	100	Ur	−9.4	12.2	10.5	257	68.4	55.3	154.1	2.8	179	0.6
		Vr	4.8	12.7								
	152	Ur	−4.9	8.7	6.5	270	50.6	20.8	98.2	4.7	165	0.6
		Vr	4.2	11.0								
	200	Ur	−1.9	5.8	3.0	281	40.5	4.5	50.1	11.1	164	0.5
		Vr	2.3	8.2								
	360	Ur	−1.2	2.0	1.3	251	9.6	0.8	4.0	5.2	3	0.5
		Vr	0.4	2.0								
	1000	Ur	−0.7	1.9	0.7	234	8.3	0.3	2.5	9.6	39	0.4
		Vr	0.1	1.3								
	1360	Ur	−1.0	2.7	1.0	227	9.0	0.5	5.5	10.2	45	0.3
		Vr	−0.1	2.0								
	1685	Ur	−1.1	2.7	1.1	224	9.7	0.6	5.5	9.8	44	0.4
		Vr	−0.1	1.8								
First half	40	Ur	−11.6	9.9	12.8	255	37.7	82.0	100.9	1.2	172	0.7
(2002/11/30–2003/8/3)		Vr	5.4	10.2								
	100	Ur	−9.1	6.8	10.0	255	35.9	50.2	47.0	0.9	98	0.8
		Vr	4.3	7.0								
	152	Ur	−3.7	3.4	4.0	251	21.5	8.0	9.8	1.2	85	0.8
		Vr	1.4	2.9								
	200	Ur	−1.0	1.6	1.1	243	7.9	0.6	2.0	3.5	58	0.6
		Vr	0.3	1.2								
	360	Ur	−0.9	1.6	0.9	238	5.9	0.4	2.0	4.6	39	0.5
		Vr	0.1	1.1								
	1000	Ur	−0.5	1.7	0.5	244	7.2	0.1	1.9	14.0	40	0.4
		Vr	0.1	1.0								
	1360	Ur	−0.9	2.7	0.9	238	8.7	0.4	5.1	12.3	40	0.3
		Vr	0.1	1.7								
	1685	Ur	−0.9	2.6	0.9	232	8.2	0.4	4.3	10.8	40	0.4
		Vr	−0.0	1.4								

Period	Mooring depth	Velocity component	Mean	SD	Vector mean			MKE	EKE	EKE/MKE	Principal axis	Direction stability
					Speed	Dir.	Max. speed					
	(m)		(cm/s)	(cm/s)	(cm/s)	(°)	(cm/s)	(cm^2/s^2)	(cm^2/s^2)		(°)	
Second half (2003/8/4–2004/4/7)	40	Ur	−12.3	20.9	12.6	241	78.7	78.6	377.7	4.8	46	0.5
		Vr	2.4	17.9								
	100	Ur	−9.7	15.8	11.0	259	68.4	60.8	260.6	4.3	1	0.5
		Vr	5.3	16.5								
	152	Ur	−6.2	11.7	9.3	278	50.6	45.6	177.4	4.2	169	0.5
		Vr	6.9	14.8								
	200	Ur	−3.4	8.0	5.3	281	40.5	14.3	90.7	6.4	168	0.5
		Vr	4.2	10.9								
	360	Ur	−1.4	2.3	1.6	258	9.6	1.3	5.9	4.6	173	0.5
		Vr	0.8	2.6								
	1000	Ur	−0.9	2.0	0.9	229	8.3	0.4	3.1	7.0	38	0.5
		Vr	0	1.5								
	1360	Ur	−1.2	2.6	1.2	220	9.0	0.7	5.8	8.3	56	0.4
		Vr	−0.2	2.2								
	1685	Ur	−1.2	2.9	1.2	219	9.7	0.8	6.5	8.6	50	0.4
		Vr	−0.2	2.2								

perature time-series showed that there was a slight increase of water temperature at 200 m in August 2003 followed by a relatively sharp temperature increase from the beginning of September to mid-October 2003 (Fig. 2). During this period northward currents between 100 and 200 m became stronger (>50 cm/s), as mentioned previously.

Sea surface temperature (SST) images in September 2003 taken in the interval between Figs. 4(e) and (g) show a warm eddy feature with cold core northeast of EC1 (Figs. 5(a) and (b)). The eddy feature is often characterized by a surface cold core wrapped by a warm streamer but with a warm subsurface core inside the eddy and a thick thermostad at the center of the eddy (Gordon *et al.*, 2002; Shin *et al.*, 2005). A similar eddy feature appears to be imprinted in the horizontal temperature distribution in August 2003 (Fig. 4(e)). The surface cold core moved to the southeast, and EC1 was now located at the western periphery of the eddy in mid-October 2003 (Fig. 5(c)). The northwestward subsurface flows between 100 and 200 m have intensified between the two periods (Figs. 2 and 4(f)). The SST image in mid-October (Fig. 5(c)) indicates that the occurrence of the eddy is associated with the westward extension of the OB. Temperatures at 200 and 360 m between mid-October and late November 2003 reached their respective maxima over the entire mooring period (Fig. 2). During this period, the center of the warm eddy was close to EC1 according to the SST image on October 31, 2003 (Fig. 5(d)), which is also evidenced by the observed weak currents during this period (Fig. 2).

Temperature at 200 m dropped sharply at the end of November 2003, and strong south or southwestward currents followed until early February 2004. The horizontal temperature distribution in December 2003 (Fig. 4(g)) showed a well-captured warm eddy feature with its center northwest of EC1. The SST image on December 21, 2003 (Fig. 5(e)) shows a warm eddy feature with cold core northwest of EC1, and the same eddy as was observed during the first warming event is thought to migrate to the northwest of EC1, resulting in the cooling of subsurface temperature and strengthening of southward currents observed at EC1.

In February 2004, an eddy feature elongated in the north-south direction was also seen in the horizontal temperature distribution at 200 m but with an increase in the core temperature as compared to that observed in December 2003 (Fig. 4(h)). The horizontal temperature gradient increased near EC1 in February 2004, and a strong southwestward current with a mean speed of 13 cm/s was observed at 200 m. The temperature time-series at 160 and 200 m indicate another warming event at 160 and 200 m between mid-January and mid-February 2004. The observed currents during this second warming event became strengthened as compared to those prior to the second

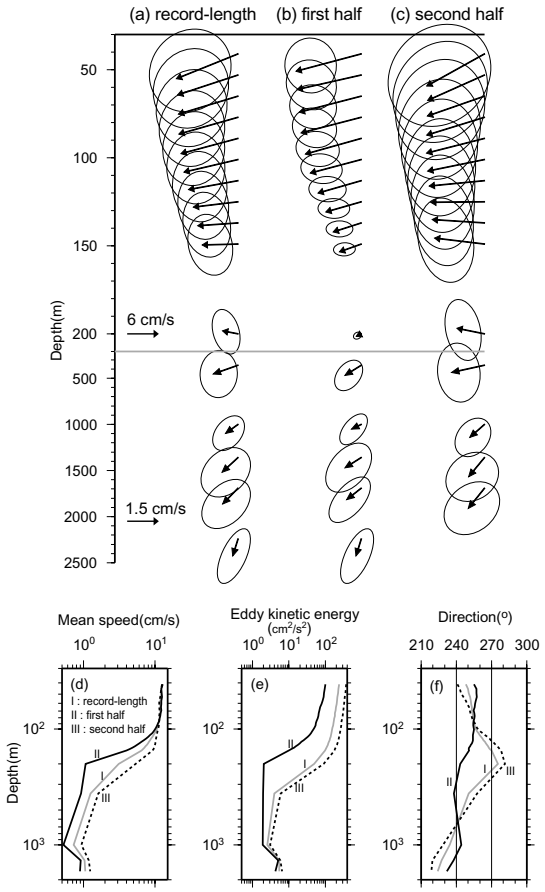

Fig. 6. Mean current vectors and their standard deviation ellipses during (a) the record-length period, (b) November 2002–early August 2003 (first half) and (c) early August 2003–April 2004 (second half). Current data at 2255 m were only available from November 2002 to June 2003. Vertical profiles of (d) mean current speed, (e) eddy kinetic energy, and (f) mean current direction during the record-length period (I), first half (II), and second half (III).

warming event, and the current direction turned from mainly southward before the event to southwestward during the second warming event. It is not clear whether the observed second warming event arose from the eastward shift of the pre-existing eddy observed in December 2003 or from other newly-developed eddies, or from changes in the upper circulation. We did not investigate this further, but it is obvious from these results that the upper currents above the pycnocline are closely related to the movement of anticyclonic warm eddies frequently reported in this region (Chang *et al*., 2004; Mitchell *et al*., 2005a).

Time-mean current vectors and their standard deviation ellipses at different depths are shown in Figs. 6(a)–(c), and basic statistics are summarized in Table 1. We divided the record-length period into two parts: a first half (8.3 months) before early August 2003 and a second half after early August 2003, considering the observed temperature and velocity time-series. The first half-period is characterized by relatively low temperature and weak currents in the upper layer, while the remaining period displays high temperature and strong currents. Record-length mean flows in the upper 200 m are directed west-south-westward or westward toward the UB with speeds ranging from 3.0 to 12.6 cm/s. Mean current speeds from 40 to 100 m change little for different averaging periods. Although current became intensified during the second half, strong northward and southward currents alternated, resulting in a weak mean current during the second half, contrasting with weaker but dominant southward currents during the first half. During the passage of the warm eddy feature, the depth of strong currents penetrates down to 360 m, hence the mean current speeds at 152 and 200 m during the second half became two or five times stronger than those during the first half (Table 1). Mean currents veer clockwise with depth during the second half in the upper layer, while they show little veering in the upper 150 m and turn anticlockwise from 150 to 200 m during the first half.

Eddy kinetic energy (EKE) in the upper 200 m during the second half is about 3 to 40 times higher than the EKE during the first half, and the ratio of EKE to mean kinetic energy (MKE) during the second half is also higher than that during the first half (Table 1). At 200 m, the EKE was 2 cm^2/s^2 during the first half, which is lower than EKE values at depth levels deeper than 1000 m, while the EKE at 200 m exceeded 90 cm^2/s^2 during the second half. Correspondingly, the standard deviation ellipses during the second half are larger than those during the first half (Figs. 6(b) and (c)).

3.2 Currents in the deep layer

Mean flows in the deep layer are directed to the southwest toward the UB with mean speeds in a range of 0.7–1.6 cm/s (Table 1 and Figs. 6(a)–(c)). The direction vector of the mean currents shows only a slight change within a 12° angle in the 685-m portion of the water column between 1000 and 1685 m, regardless of the averaging periods (Fig. 6(f)). During the first half, the direction between 200 and 1685 m changed within only a 12° angle, and the change of direction with depth was irregular. However, the change in the mean current direction between 360 and 1000 m became larger at about a 40° angle during the second half, and the mean current direction veered counterclockwise with depth in the deep layer. The flows at 360 m were sometimes in the opposite direction to those in the deeper depth levels when strong upper flows extending down to 200 m occurred in October 2003 (Fig. 2).

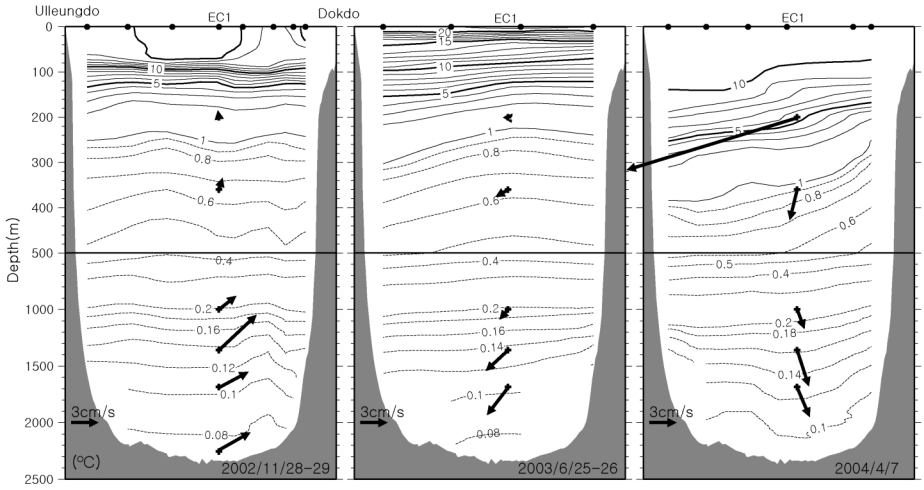

Fig. 7. Vertical sections of potential temperature in (a) November 2002, (b) June 2003, and (c) April 2004 in the Ulleung Interplain Gap†. The 5-day averaged mean current vectors observed at EC1 around the time of CTD surveys are shown.

One of the most notable characteristics of deep flows is the existence of the minimum kinetic energy level in the deep layer. The MKE, EKE, and mean speed at 1000 m are smaller than those at 360 and 1685 m in both the first and second periods (Table 1, Figs. 6(d) and (e)), implying the existence of bottom-intensified mean currents and current fluctuations below 1000 m depth. This is also obvious in the time-series of low-passed current vectors in Fig. 2. Between January and March 2003, deep currents below 1360 m were even stronger than the current at 200 m.

Figure 7 shows the vertical distribution of potential temperature in November 2002, June 2003, and April 2004 taken during the period of the moored current observation at EC1. Also shown are 5-day averaged mean currents below 200 m around the time of each CTD survey. The 5-day averaging period is based on the integral timescales of deep currents, ranging between 4–9 days. Although the direction of deep currents varies depending on the observation periods, the current at 1000 m was weaker than the currents at greater depths and also weaker than currents at 360 m in June 2003 and April 2004. The horizontal slope of isotherms decreases with depth, becoming nearly flat approximately between 600 and 1100 m. The slope increases again below 1200 m.

The mean current speed and EKE in the deep layer increased during the second half as compared with those during the first half (Figs. 6(d) and (e)). The rate of the increase in the EKE, however, is smaller than that in the MKE (Table 1), hence the EKE/MKE ratio reduced during the second half, suggesting that energetic current fluctuations below the permanent thermocline are not directly related to those in the upper layer, which arose mainly from the passage of the mesoscale eddy. This can also be seen in the time-series of vector currents (Fig. 2).

3.3 Spectral characteristics

To investigate dominant timescales of current fluctuations, power spectra of Ur and Vr velocity components are calculated in variance-preserving form using their record-length time-series shown in Fig. 3. Below 360 m, the power spectra for both Ur and Vr components show a predominant peak at an approximately 40-day period, with the minimum energy level at 1000 m (Fig. 8). The 40-day spectral energy levels at 1360 and 1685 m are higher than those at 200 and 360 m depths, suggesting that the flow variability intensifies with depth. The 40-day-period spectral energy levels for Ur are greater than those Vr except at 1360 m, suggesting that the 40-day-period current fluctuations in the deep layer mainly occur in the along-channel direction.

In the upper 200 m, the power spectra for Ur show high energy levels at 5–20 days at 40 m and near 60 days at 100 and 152 m. For Vr, the power spectra above 100 m peak at roughly 50 days, whereas the spectra at 152 and 200 m have high energy levels at periods longer than approximately 80 days. In the upper 100 m, spectral energy at around 50–60 days for Vr is higher than that for Ur. The Vr component in the upper 100 m shows alternating current directions on timescales of about 50–60 days, while the sign of Ur in the upper layer changes little (see Fig. 3). This suggests that current fluctuations with a period range of 50–60 days occur mainly in the cross-channel direction in the upper 100 m, in contrast to the dominant fluctuations in the along-channel direction in the deep layer. In the upper 200 m, the energy levels at 40-day

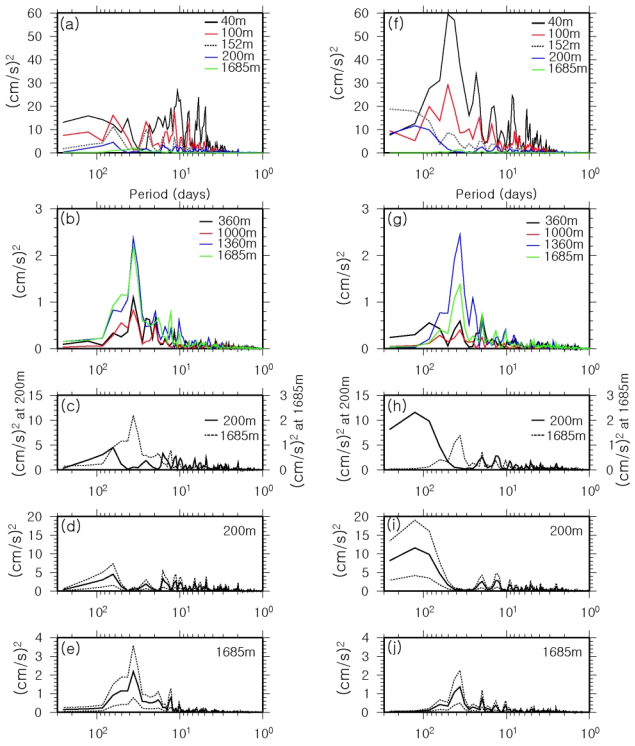

Fig. 8. Variance-preserving power spectra for along-channel (Ur, left panels) and cross-channel components (Vr, right panels) of low-pass filtered currents. Dashed lines in the lower four panels show the 95% confidence limits at some selected depth levels. Note the different vertical scale at (c) and (h).

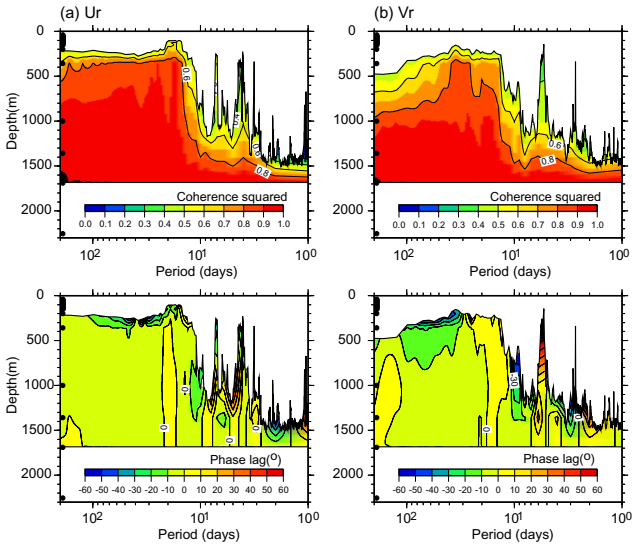

Fig. 9. Contour maps of the coherence squared (upper panel) and phase lag (lower panel) between 1685 m and shallower depth levels for (a) along-channel (Ur) and (b) cross-channel components (Vr) of low-pass filtered currents. A positive phase indicates that currents at 1685 m lag those at shallower depths. The region below the 95% confidence level is omitted in the contouring. Instrument depths are shown with black dots at the left side of each figure.

period for both Ur and Vr, which is the dominant period in the deep layer, decrease significantly with depth, and the energy at 200 m becomes lower than that at 1685 m. Therefore, it is difficult to combine the 40-day variability in the deep layer with that in the upper 100 m.

To better understand the vertical structure of the flow variability, the coherence squared between 1685 m and shallower depth levels is calculated and shown as a composite map (Fig. 9). For a period range of 15–100 days, the coherence squared between 1685 m and shallower depths up to 360 m exceeds the 95% confidence level with nearly zero phase lag for both velocity components. The coherence squared for a period of 15–20 days for Ur exceeded the 95% confidence level up to 100 m. For periods shorter than 15 days, the statistically significant coherence exceeding the 95% confidence level occurs only around 4 and 7 days for Ur and around 5 days for Vr.

As mentioned in Subsection 3.1, the current meter at 200 m was mostly located below the permanent thermocline during the first half of the entire mooring period, while it was mainly located within the permanent thermocline during the second half due to the deepening of the thermocline associated with the passage of the anticyclonic mesoscale eddy. The coherence squared for Ur between 200 and 1685 m during the first period exceeds the 95% confidence level with nearly zero phase lag for periods longer than 15 days, while the coherence between the two depths falls below the 95% confidence level during the second period (not shown), implying that deep current fluctuations below the permanent thermocline are nearly depth-independent for periods longer than approximately 15 days, while the deep current fluctuations are not correlated with those in the depth levels above the permanent pycnocline.

3.4 Modal structure

EOF analyses are applied to the low-passed 12-hourly time series of Ur and Vr in order to examine the predominant vertical structure and its temporal variation. The observed data significantly straddle through the entire water column and EOF analyses are performed separately for upper (40–200 m) and deep (360–1685 m) layers. The relation of current fluctuations between the upper and deep layers is then investigated by comparing time coefficients of leading EOF modes for the upper and deep layers. Figures 10 and 11 show the amplitudes and time coefficients of two leading EOF modes for each layer. The first and second modes together explain more than

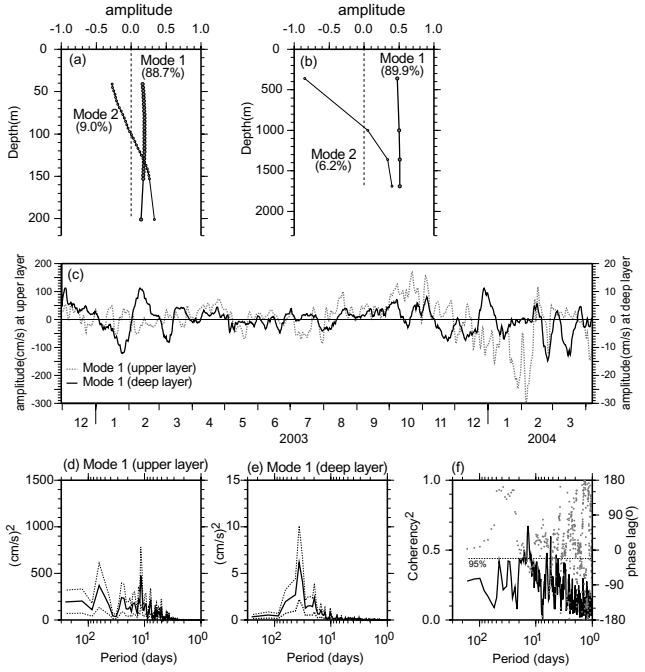

Fig. 10. Vertical structure of EOF modes (a, b), time coefficients of the first EOF mode (c), variance-preserving power spectra (d, e), and coherency and phase lag between upper and deep layers for time coefficients of the first EOF mode (f) for the along-channel velocity component (Ur). (a) and (d) for the upper layer, and (b) and (e) for the deep layer. Dashed lines in (d) and (e) denote the 95% confidence limits, and dots and dashed line in (f) show the phase lag and the 95% confidence level, respectively.

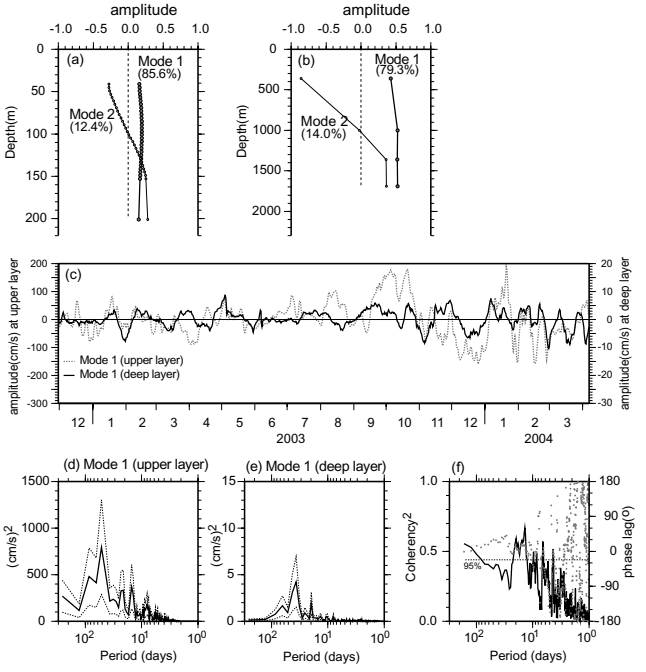

Fig. 11. The same as Fig. 10, except for the cross-channel velocity component (Vr).

93% of total variances for Ur and Vr both in the upper and deep layers (Figs. 10(a), 10(b), 11(a), 11(b)). In the deep layer the second mode is not statistically significant according to our criterion given in Section 2.

The first EOF modes for both the upper and deep layers are characterized by nearly depth-independent eigenvectors and explain more than 79% of the total variance for both Ur and Vr. The first EOF mode in the deep layer has minimum amplitude at 360 m, especially for Vr (Fig. 11(b)). The second modes for both Ur and Vr have nodal points at 100 m in the upper layer and 1000 m in the deep layer, and represent the out-of-phase current fluctuations above and below the nodal points. The nodal point at 1000 m in the deep layer corresponds to the minimum EKE at this depth level. The second modes explain more than 6.2% of total variances for both velocity components in the upper and deep layers, and the contribution of the second mode for Vr (>12.4%) to total variances is more pronounced as compared to that for Ur.

Spectral analyses of the first mode in the upper layer show high energy level near 12, 25, and 64 days for Ur (Fig. 10(d)), 15, 21, and 51 days for Vr (Fig. 11(d)). The spectral peaks for the first mode in the upper layer are similar to those of current spectra above 100 m (Fig. 8(a)). The power spectra of the first mode in the deep layer show a predominant peak at an approximately 40-day period with a secondary peak at about a 20-day period (Figs. 10(e) and 11(e)), similar to the current spectra in the deep layer (Fig. 8(b)). Time coefficients of the first EOF modes in the upper and deep layers are poorly correlated for both velocity components (Figs. 10(c) and 11(c)) with cross-correlation coefficients less than 0.1 and 0.18 for Ur and Vr, respectively. The squared coherences computed using two pairs of time coefficient data shown in Figs. 10(c) and 11(c) do not exceed the 95% confidence level for a period range of 23–70 days, indicating that the dominant 40-day current fluctuations in the deep layer are not related to the upper current variability (Figs. 10(f) and 11(f)). The squared coherences exceed the 95% confidence level for 12–16 days for Ur and for 12–22 days for Vr. Cross-correlation coefficients for other pairs of time coefficients of different modes in the upper and deep layers are insignificant.

3.5 Summary of results

The full-depth current measurement at EC1 in the middle of the Ulleung Interplain Gap between November 2002 and April 2004 has revealed some details of the vertical structure of low-frequency currents.

Record-length mean currents are directed towards the

Ulleung Basin throughout the entire water column with speeds of 6.5 to 12.6 cm/s between 40 m and 152 m, and 0.7 to 3.0 cm/s at and below 200 m. The mooring site EC1 was affected by the westward migrating anticyclonic warm eddy feature during the second half of the observation period. SST images and subsurface CTD data suggest the eddy generation was associated with the westward extension of the Offshore Branch. An increase in the subsurface temperature was observed during this period down to at least 360 m. The temperature increase reached about 6°C at 160 m. Upper currents responded to the passage of the eddy, and an intensification of northwestward (>51 cm/s) and southwestward (>78 cm/s) upper currents occurred when EC1 was placed near the western and eastern side of the eddy feature, respectively. When EC1 was close to the center of the eddy, a thermostad developed and upper currents became weak. During the warming period in the second half of the observation period, strong currents developed down to 360 m. Currents at even greater depths seems to be partly affected by the passage of the eddy. Southwestward deep currents were dominant during the observation period, while weak northward currents occurred when the upper currents flowed strongly northward.

The characteristics of the observed deep currents below the permanent thermocline from 360 m down to the bottom can be summarized as follows: 1) inflow toward the Ulleung Basin with a maximum speed of 10 cm/s; 2) minimum kinetic energy level at 1000 m; 3) predominance of approximately 40-day variability; 4) nearly depth-independent current fluctuation below the permanent pycnocline down to the bottom with nearly zero phase lag for periods longer than approximately 15 days.

The 40-day variability, which is dominant both in along-channel and cross-channel velocity components of the deep layer, is not obvious in the along-channel component of the upper currents. The cross-channel component of upper currents also contains a relatively large energy at 40-day period, but the spectral energy has a maximum value in the uppermost currents at 40 m and reduces greatly with depth. The spectral energy at 40-day variability at 200 m is lower than that at 1685 m.

More than 79% of variances of current fluctuations in the upper and deep layers are explained by their respective first EOF modes characterized by nearly depth-independent eigenvectors. The time coefficients of the first modes in the upper and deep layers, however, correlated poorly at a 40-day period, which is a dominant time scale for current fluctuations in the deep layer. Depth-independent current fluctuations in the upper and deep layers are shown to be significantly correlated in a period range between 12–22 days, but the spectral analyses show much reduced spectral energy in this period range for deep currents.

4. Discussion

The observed deep currents showed a predominance of southwestward flows toward the Ulleung Basin. Chang *et al*. (2002a, 2004) also reported southwestward mean flows below 400 m at EC1 during November 1996–May 2002. Hence, the southwestward mean flows in the deep layer at EC1 are robust. One of the new findings of the present, denser mooring data, however, is that both the mean and fluctuating currents show minima at 1000 m. Previous current measurements at EC1, taken at three nominal depths around 400, 1400, and 20 m above the bottom, showed the minimum current either at 400 or 1400 m (Chang *et al*., 2002a, 2004). Vertical temperature sections taken during the mooring period show that isotherm slopes become nearly flat at approximately 1000 m, and they become steeper with depth below 1000 m. This suggests that the reference level at around 1000 m for geostrophic current calculation in the UIG is more realistic than that at other depths.

Below 1000 m, the currents become intensified, and the EOF analyses confirm that dominant deep current fluctuations are not directly related to local upper current variability. Intensified flows in the deep layer or near the bottom were also observed over the sloping topography of the UB (station D6 of Senjyu *et al*., 2005) and Yamato Basin (station C5 of Senjyu *et al*., 2005). Therefore, intensified flows in the deep layer may occur extensively in the East Sea, especially over regions of sloping topography. Such deep-layer-intensified flows may play an important role in the deep circulation of the East Sea because of their energetic characteristics.

An important finding from this observation is the poor relation between the current fluctuations in the upper and deep layers, at least during the period of moored current measurement. The upper currents became energetic during the passage of a warm eddy feature, and mean current speeds in the upper layer increased substantially during this period as compared to those during the first half of the total period. The eddy kinetic energy in the deep layer, however, increased only slightly, while the ratio of the mean and eddy kinetic energy decreased during the second half of the total period. A linkage between upper currents and the deep currents was found in September and October 2003, when strong northward currents developed between 100 and 200 m. During that time, weak and northward deep currents occurred instead of dominant southwestward currents. As only one (or two) passage of the eddy feature was detected, it is inconclusive whether the surface eddy activities influence currents in the deep layer.

Takematsu *et al*. (1999) discussed the relationship between the upper layer anticyclonic eddies and deep currents in the Japan Basin Interior. They showed that anticyclonic eddies revealed by SST images and drifter

tracks are well correlated with the vertically coherent deep currents. Takematsu *et al*. (1999), however, mentioned that this was not the case in the spring season, and their comparison between SST images and current data was all done in the cold season, when the vertical stratification is weak. The discrepancy between our result and that of Takematsu *et al*. (1999) needs to be further elucidated, and we conjecture that the poor relationship between upper and deep currents in the Ulleung Interplain Gap is due to stronger stratification in the southwestern East Sea, and an excitation of the 40-day variability in the deep layer that is indistinct in the upper currents.

The development of a thick thermostad in the upper layer would shrink the thickness of deep layer, resulting in the generation of an anticyclonic vorticity. A single mooring would not be enough to clarify this dynamic consequence. Recently, a successful observation of the abyssal layer below 1800 m throughout the entire UIG has been accomplished (Chang *et al*., 2009), and analyses of the spatial structure across the entire UIG are required to clarify deep flow variability at EC1.

Acknowledgements

The authors thank Mr. Sang-Chul Hwang, Mr. Yong-Suk Jang and Dr. Moon-Bo Shim as well as the officers and crews of R.V. *Eardo*, *HaeYang2000* and *TamYang* for their dedication and support during the mooring work. This paper was written with support from the Ministry of Land, Transport and Maritime Affairs (the Korean EAST-I program of CREAMS/PICES) and the Korea Research Foundation Grant funded by the Korean Government (MOEHRD, Basic Research Promotion Fund) (KRF-2006-311-C00619). The first author was partly supported by the Ministry of Education, Science Technology, Korea through project BK21.

References

Chang, K.-I., N. G. Hogg, M.-S. Suk, S.-K. Byun, Y.-G. Kim and K. Kim (2002a): Mean flow and variability in the southwestern East Sea. *Deep-Sea Res. I*, **49**, 2261–2279.

Chang, K.-I., Y.-B. Kim, M.-S. Suk and S.-K. Byun (2002b): Hydrography around Dokdo. *Ocean and Polar Res*., **24**(4), 369–389.

Chang, K.-I., W. J. Teague, S. J. Lyu, H. T. Perkins, D.-K. Lee, D. R. Watts, Y.-B. Kim, D. A. Mitchell, C. M. Lee and K. Kim (2004): Circulation and currents in the southwestern East/Japan Sea: overview and review. *Prog. Oceanogr*., **61**, 105–156.

Chang, K.-I., K. Kim, Y.-B. Kim, W. J. Teague, J.-C. Lee and J.-H. Lee (2009): Deep flow and transport through the Ulleung Interplain Gap in the southwestern East/Japan Sea. *Deep-Sea Res. I*, **56**, 61–72.

Gordon, A. L., C. F. Giulivi, C. M. Lee, H. H. Furey, A. Bower and L. Tally (2002): Japan/East Sea Intrathermocline Eddies. *J. Phys. Oceanogr*., **32**, 1960–1974.

Kim, K., K.-R. Kim, J. Y. Chung and H. S. Yoo (1991): Characteristics of physical properties in the Ulleung Basin. *J. Oceanol. Soc. Korea*, **26**, 83–100.

Kim, K., K.-R. Kim, Y.-G. Kim, Y.-K. Cho, D.-J. Kang, M. Takematsu and Y. Volkov (2004): Water mass and decadal variability in the East Sea (Sea of Japan). *Prog. Oceanogr*., **61**, 157–174.

Kundu, P. K., J. S. Allen and R. L. Smith (1975): Modal decomposition of the velocity field near the Oregon coast. *J. Phys. Oceanogr*., **5**, 683–704.

Mitchell, D. A., D. R. Watts, M. Wimbush, W. J. Teague, K. L. Tracey, J. W. Book, K.-I. Chang, M.-S. Suk and J.-H. Yoon (2005a): Upper circulation patterns in the Ulleung Basin. *Deep-Sea Res. II*, **52**, 1617–1638.

Mitchell, D. A., W. J. Teague, M. Wimbush, D. R. Watts and G. G. Sutyrin (2005b): The Dok Cold Eddy. *J. Phys. Oceanogr*., **35**, 273–288.

North, G. R., T. L. Bell, R. F. Cahalan and F. J. Moeng (1982): Sampling errors in the estimation of empirical orthogonal functions. *Mon. Wea. Rev*., **110**, 699–706.

Overland, J. E. and R. W. Preisendorfer (1982): A significance test for principal components applied to a cyclone climatology. *Mon. Wea. Rev*., **110**, 1–4.

Preisendorfer, R. W. (1988): *Principal Component Analysis in Meteorology and Oceanography*, ed. by C. D. Mobley, Elsevier Science Publishers B.V., New York, 425 pp.

Senjyu, T., H.-R. Shin, J.-H. Yoon, Z. Nagano, H.-S. An, S.-K. Byun and C.-K. Lee (2005): Deep flow field in the Japan/East Sea as deduced from direct current measurements. *Deep-Sea Res. II*, **52**, 1726–1741.

Shin, H.-R., C.-W. Shin, C. Kim, S.-K. Byun and S.-C. Hwang (2005): Movement and structural variation of warm eddy WE92 for three years in the western East/Japan Sea. *Deep-Sea Res. II*, **52**, 1742–1762.

Takematsu, T., A. G. Ostrovskii and Z. Nagano (1999): Observations of eddies in the Japan Basin interior. *J. Oceanogr*., **55**, 237–246.

Teague, W. J., K. L. Tracey, D. R. Watts, J. W. Book, K.-I. Chang, P. J. Hogan, D. A. Mitchell, M.-S. Suk, M. Wimbush and J.-H. Yoon (2005): Observed deep circulation in the Ulleung Basin. *Deep-Sea Res. II*, **52**, 1802–1826.